INTERNATIONAL JOURNAL FOR NUMERICAL METHODS IN FLUIDS
Int. J. Numer. Meth. Fluids 2000; **32**: 51–78

A new finite element formulation for both compressible and nearly incompressible fluid dynamics

P.A.B. De Sampaio* and M.L. Moreira

Instituto de Engenharia Nuclear, Comissão Nacional de Energia Nuclear, Cidade Universitaria, Ilha do Fundao, CEP 21945-970, CP 68550, Rio de Janeiro-RJ, Brazil

SUMMARY

A new finite element formulation designed for both compressible and nearly incompressible viscous flows is presented. The formulation combines conservative and non-conservative dependent variables, namely, the mass–velocity (density∗velocity), internal energy and pressure. The central feature of the method is the derivation of a discretized equation for pressure, where pressure contributions arising from the mass, momentum and energy balances are taken implicitly in the time discretization. The method is applied to the analysis of laminar flows governed by the Navier–Stokes equations in both compressible and nearly incompressible regimes. Numerical examples, covering a wide range of Mach number, demonstrate the robustness and versatility of the new method. Copyright © 2000 John Wiley & Sons, Ltd.

KEY WORDS: finite element formulation; compressible flow; nearly incompressible flow; mass–velocity

1. INTRODUCTION

Most numerical methods for the analysis of compressible fluid dynamics present difficulties when applied to low-speed (nearly incompressible) flow problems. The difficulties originate from the fast propagation of pressure waves, as flow conditions approach the incompressible limit. In such cases, the accurate representation of pressure transients requires the use of extremely small time steps, which are unaffordable in practical applications. Conversely, the use of time steps larger than the typical pressure time scale results in errors that may lead to numerical instability. In particular, if an explicit time approximation of pressure is adopted—a usual choice in algorithms for high-speed compressible flows—such errors grow during the computation and stability is rapidly lost.

Nearly incompressible flows, i.e. flows characterized by very small Mach number, are usually approximated as fully incompressible. Thus, compressibility effects are eliminated from the start, at the modelling level, prior to considering any particular discretization method. This

* Correspondence to: Instituto de Engenharia Nuclear, Comissão Nacional de Energia Nuclear, Cidade Universitaria, Ilha do Fundao, CEP 21945-970, CP 68550, Rio de Janeiro-RJ, Brazil.

CCC 0271–2091/2000/010051–28$17.50

Received March 1998
Revised July 1998

is achieved by a change of the physical and mathematical model, where the original mass conservation law and state equation are replaced by the incompressibility constraint, requiring the velocity field to be divergence-free. In such a context, pressure is no longer a thermodynamic property related to density through a state equation. Most importantly, the pressure hyperbolic character and the associated wave-like pressure propagation disappear from the model. Instead, in a fully incompressible flow, pressure takes an elliptic character: it must be determined from the momentum balance and boundary conditions in such a way that the incompressibility constraint ($\nabla \cdot \mathbf{u} = 0$) is enforced at all times.

Because of these distinct mathematical characters, i.e. hyperbolic versus elliptic pressure behaviour, it is not surprising that methods for the discretization of compressible and incompressible flows have developed independently and, to some extent, apart. The computational fluid dynamics (CFD) literature reflects this dichotomy and most papers are devoted specifically to either compressible or incompressible fluid flow applications. Only recently has the literature clearly indicated the interest in numerical schemes appropriate to all speed regimes. The development of methods for a wide range of Mach numbers is welcome to the analysis of many flow problems involving simultaneously both the compressible and the nearly incompressible behaviour. In fact, even in the high-speed compressible flows of the aerospace industry, the nearly incompressible behaviour is present near solid walls and leading edges.

Different approaches have been pursued in the development of methods for all-speed fluid flows. Karki and Patankar [1] and Maliska and Silva [2] introduced finite volume pressure based methods obtained through the extension of schemes originally developed for incompressible problems. The works of Chen and Pletcher [3] and Azevedo and Martins [4] are examples of classical finite volume compressible methods modified in order to deal with incompressible flows. In the finite element context, Zienkiewicz and Codina [5] used fractional steps and characteristic Galerkin approximations to derive their all-speed formulation.

In this paper, a unified treatment for the analysis of both compressible and nearly incompressible flows is presented. Although the discussion has been restricted to laminar flows governed by the Navier–Stokes equations, the methodology proposed can be readily extended to accommodate the Reynolds-averaged equations and turbulence closure models. The formulation is written combining conservative and non-conservative dependent variables. These are the mass–velocity vector (density$*$velocity), internal energy and pressure. Linear finite elements are used to approximate the field variables.

An important feature of the method is the implicit time discretization of the mass balance and of the pressure terms appearing in the momentum and energy equations. Petrov–Galerkin weighting functions, derived from a least-squares procedure, are employed in the momentum- and energy-weighted residual statements. The resulting formulation automatically introduces *streamline upwinding* [6] and pressure stabilizing terms. Moreover, the method retains stability, despite ignoring the short time scales associated with the fast pressure transients of nearly incompressible flows.

Numerical examples are presented. Steady and unsteady flow simulations, covering a wide range of Mach numbers, demonstrate the robustness and versatility of the new method.

2. THE CONTINUUM MODEL

We present here the continuum model used in our description of compressible viscous flows. The problem is defined on the open bounded domain Ω, with boundary Γ, contained in the *nsd*-dimensional Euclidean space. The governing equations are written using the summation convention for $a = 1, \ldots, nsd$ and $b = 1, \ldots, nsd$, in Cartesian co-ordinates, as

Conservation of mass

$$\frac{\partial \rho}{\partial t} + \frac{\partial G_a}{\partial x_a} = 0. \tag{1}$$

Conservation of momentum

$$\frac{\partial G_a}{\partial t} + u_b \frac{\partial G_a}{\partial x_b} + \frac{\partial u_b}{\partial x_b} G_a - \frac{\partial \tau_{ab}}{\partial x_b} + \frac{\partial p}{\partial x_a} - \rho g_a = 0. \tag{2}$$

Conservation of energy

$$\rho\left(\frac{\partial e}{\partial t} + u_b \frac{\partial e}{\partial x_b}\right) + p \frac{\partial u_b}{\partial x_b} + \frac{\partial q_b}{\partial x_b} - \tau_{ab} \frac{\partial u_a}{\partial x_b} = 0. \tag{3}$$

Constitutive equations for viscous stress and heat flux

$$\tau_{ab} = -\frac{2}{3}\mu\left(\frac{\partial u_c}{\partial x_c}\right)\delta_{ab} + \mu\left(\frac{\partial u_a}{\partial x_b} + \frac{\partial u_b}{\partial x_a}\right), \tag{4}$$

$$q_b = -\kappa \frac{\partial T}{\partial x_b}. \tag{5}$$

Thermodynamics (ideal gas)

$$p = (\gamma - 1)\rho e, \tag{6}$$

$$e = c_v T, \tag{7}$$

$$\gamma = \frac{c_p}{c_v}. \tag{8}$$

In the above equations u_a, p, e, ρ and T denote the velocity, pressure, internal energy, density and temperature fields respectively. The mass–velocity (density$*$velocity) is represented by $G_a = \rho u_a$. The gravity field is g_a. The symbols μ, κ, c_v and c_p represent the fluid properties of viscosity, thermal conductivity, specific heat at constant volume and specific heat at constant pressure respectively.

Note that using the mass balance (1) and the state equation (6), the energy equation (3) can be alternatively written as

$$\gamma\rho\left(\frac{\partial e}{\partial t}+u_b\frac{\partial e}{\partial x_b}\right)+\frac{\partial q_b}{\partial x_b}-\tau_{ab}\frac{\partial u_a}{\partial x_b}=\frac{\partial p}{\partial t}+u_b\frac{\partial p}{\partial x_b}. \tag{9}$$

The above form of the energy equation will be also used in the derivations presented in the next section.

2.1. Using the state equation to eliminate density

The governing equations can be recast as follows, where density is eliminated from the mass balance and the gravity field potential φ is introduced:

Conservation of mass

$$\alpha\frac{\partial p'}{\partial t}-\beta\frac{\partial e}{\partial t}+(1+\alpha\varphi)\frac{\partial G_a}{\partial x_a}=0. \tag{10}$$

Conservation of momentum

$$\frac{\partial G_a}{\partial t}+u_b\frac{\partial G_a}{\partial x_b}+\frac{\partial u_b}{\partial x_b}G_a-\frac{\partial \tau_{ab}}{\partial x_b}+\left(\frac{1}{1+\alpha\varphi}\right)\frac{\partial p'}{\partial x_a}-\left(\frac{\alpha\varphi}{1+\alpha\varphi}\right)\rho g_a+\left(\frac{\beta\varphi}{1+\alpha\varphi}\right)\frac{\partial e}{\partial x_a}=0. \tag{11}$$

Conservation of energy

$$\rho\left(\frac{\partial e}{\partial t}+u_b\frac{\partial e}{\partial x_b}\right)+(p'+p_0-\rho\varphi)\frac{\partial u_b}{\partial x_b}+\frac{\partial q_b}{\partial x_b}-\tau_{ab}\frac{\partial u_a}{\partial x_b}=0, \tag{12}$$

or, corresponding to Equation (9),

$$\begin{aligned}&\gamma\rho\left(\frac{\partial e}{\partial t}+u_b\frac{\partial e}{\partial x_b}\right)+\frac{\partial q_b}{\partial x_b}-\tau_{ab}\frac{\partial u_a}{\partial x_b}\\&=\frac{\partial p'}{\partial t}+\left(\frac{1}{1+\alpha\varphi}\right)u_b\frac{\partial p'}{\partial x_b}+\left(\frac{1}{1+\alpha\varphi}\right)G_b g_b+\left(\frac{\beta\varphi}{1+\alpha\varphi}\right)u_b\frac{\partial e}{\partial x_b}+\varphi\frac{\partial G_b}{\partial x_b}.\end{aligned} \tag{13}$$

The modified pressure p', the gravity field potential φ and the thermodynamic properties α and β are given by

$$p'=p-p_0+\rho\varphi, \tag{14}$$

$$\varphi=-\mathbf{g}\cdot\mathbf{x}=-g_b x_b, \tag{15}$$

$$\alpha = \left(\frac{\partial \rho}{\partial p}\right)_e = \frac{1}{(\gamma - 1)e} = \frac{\rho}{p}, \tag{16}$$

$$\beta = -\left(\frac{\partial \rho}{\partial e}\right)_p = \frac{p}{(\gamma - 1)e^2} = \frac{\rho}{e}, \tag{17}$$

and p_0 is the reference pressure for the problem at hand.

2.2. Governing equations in non-dimensional form

Let us define non-dimensional variables, denoted with an asterisk *, which are related to the original dimensional variables according to

$$\begin{array}{llll} u_a = u_0 u_a^*, & p' = \rho_0 u_0^2 p^*, & T = T_0(T^* + 1), & G_b = \rho_0 u_0 G_b^*, \\ e = e_0(e^* + 1), & \rho = \rho_0 \rho^*, & \varphi = |\mathbf{g}| L \varphi^*, & g_a = |\mathbf{g}| g_a^*, \\ \mu = \mu_0 \mu^*, & \kappa = \kappa_0 \kappa^*, & x_a = L x_a^*, & t = L t^*/u_0, \\ \alpha = \alpha^*/u_0^2, & \beta = \beta^* \rho_0 / e_0, & & \end{array} \tag{18}$$

where the subscript zero '0' indicates reference values and L is the reference length. In terms of the non-dimensional variables, the governing equations become

Mass conservation

$$\alpha^* \frac{\partial p^*}{\partial t^*} - \beta \frac{\partial e^*}{\partial t^*} + \left(1 + \frac{\alpha^* \varphi^*}{Fr^2}\right) \frac{\partial G_a^*}{\partial x_a^*} = 0. \tag{19}$$

Momentum conservation

$$\frac{\partial G_a^*}{\partial t^*} + u_b^* \frac{\partial G_a^*}{\partial x_b^*} + \frac{\partial u_b^*}{\partial x_b^*} G_a^* - \frac{1}{Re} \frac{\partial \tau_{ab}^*}{\partial x_b^*} + (1 - \Phi_1) \frac{\partial p^*}{\partial x_a^*} - \frac{\Phi_1}{Fr^2} \rho^* g_a^* + \Phi_2 \frac{\partial e^*}{\partial x_a^*} = 0. \tag{20}$$

Energy conservation

$$\rho^* \left(\frac{\partial e^*}{\partial t^*} + u_b^* \frac{\partial e^*}{\partial x_b^*}\right) + \left[\gamma - 1 + \gamma Ec p^* - \frac{\gamma Ec}{Fr^2} \rho^* \varphi^*\right] \frac{\partial u_b^*}{\partial x_b^*} + \frac{\gamma}{RePr} \frac{\partial q_b^*}{\partial x_b^*} - \frac{\gamma Ec}{Re} \tau_{ab}^* \frac{\partial u_a^*}{\partial x_b^*} = 0, \tag{21}$$

or, corresponding to Equation (13)

$$\begin{aligned} &\gamma \rho^* \left(\frac{\partial e^*}{\partial t^*} + u_b^* \frac{\partial e^*}{\partial x_b^*}\right) + \frac{\gamma}{RePr} \frac{\partial q_b^*}{\partial x_b^*} - \frac{\gamma Ec}{Re} \tau_{ab}^* \frac{\partial u_a^*}{\partial x_b^*} \\ &= \gamma Ec \left[\frac{\partial p^*}{\partial t^*} + (1 - \Phi_1) u_b^* \frac{\partial p^*}{\partial x_b^*} + \left(\frac{1 - \Phi_1}{Fr^2}\right) G_b^* g_b^* + \Phi_2 u_b^* \frac{\partial e^*}{\partial x_b^*} + \frac{\varphi^*}{Fr^2} \frac{\partial G_b^*}{\partial x_b^*}\right], \end{aligned} \tag{22}$$

where

$$\Phi_1 = \frac{\alpha^*\varphi^*}{Fr^2 + \alpha^*\varphi^*}, \tag{23}$$

$$\Phi_2 = \frac{\beta^*\varphi^*}{Fr^2 + \alpha^*\varphi^*}, \tag{24}$$

$$\tau^*_{ab} = -\frac{2}{3}\mu^*\left(\frac{\partial u^*_c}{\partial x^*_c}\right)\delta_{ab} + \mu^*\left(\frac{\partial u^*_a}{\partial x^*_b} + \frac{\partial u^*_b}{\partial x^*_a}\right), \tag{25}$$

$$q^*_b = -\kappa^*\frac{\partial T^*}{\partial x^*_b}, \tag{26}$$

$$\rho^* = \frac{\lfloor \gamma - 1 + \gamma Ecp^* \rfloor}{\left[(\gamma-1)(e^*+1) + \dfrac{\gamma Ec}{Fr^2}\varphi^*\right]}, \tag{27}$$

$$e^* = T^*, \tag{28}$$

and the non-dimensional groups of Reynolds, Froude, Prandtl and Eckert are given respectively by

$$Re = \frac{\rho_0 u_0 L}{\mu_0}, \qquad Fr = \frac{u_0}{\sqrt{|\mathbf{g}|L}}, \qquad Pr = \frac{\mu_0 c_p}{\kappa_0}, \qquad Ec = \frac{u_0^2}{c_p T_0}. \tag{29}$$

Remarks

(1) In aeronautical applications it is usual to parameterize problems using the Mach number M rather than the Eckert number Ec. For ideal gases, the relationship between these non-dimensional groups is

$$Ec = (\gamma - 1)M^2. \tag{30}$$

(2) In free convection applications, problem data usually include a reference temperature difference $\Delta\theta$ rather than a reference velocity u_0. However, it is a simple matter to define a reference velocity u_0 using the given $\Delta\theta$ and the fluid volumetric thermal expansion coefficient β_v. Indeed, if the reference velocity u_0 is chosen as $u_0 = (\beta_v \Delta\theta |\mathbf{g}| L)^{1/2}$, then the squared Reynolds number becomes the Grashof number, $Gr = Re^2 = \rho_0^2 |\mathbf{g}| \beta_v \Delta\theta L^3/\mu_0^2$, which is a non-dimensional group usually employed to parameterize free convection problems.

In the remainder of this work we shall deal exclusively with the non-dimensionalized equations and the asterisk *—used to indicate non-dimensional quantities—will be dropped.

3. THE DISCRETIZATION AND SOLUTION SCHEMES

Linear Lagrangian finite elements are employed to represent the mass–velocity, pressure and internal energy fields. The central feature of the method is the derivation of a discretized equation for pressure, where pressure contributions arising from the mass, momentum and energy balances are taken implicitly in the time discretization. The Galerkin method is used to obtain the discretized pressure equation, while a Petrov–Galerkin/least-squares based approach is used in the derivation of the discretized equations for mass–velocity and internal energy.

The problem is solved using a segregated solution procedure. Once the pressure field is found, the algorithm proceeds with the computation of the mass–velocity and internal energy fields. The cyclic update of pressure, mass–velocity and internal energy requires the solution of symmetric systems of equations. This is accomplished with preconditioned conjugate gradient solvers, suitable for parallel and vector implementation on supercomputers [7].

3.1. The equation for pressure

Let us consider the following time discretization of the mass balance (19),

$$\alpha^n\left(\frac{p^{n+1}-p^n}{\Delta t}\right)-\frac{\beta^n}{\rho^{n+1/2}}\left[\rho^{n+1/2}\left(\frac{e^{n+1}-e'}{\Delta t}\right)\right]+\frac{\partial G_a^{n+1}}{\partial x_a}$$
$$=\frac{\beta^n}{\rho^{n+1/2}}\left[\rho^{n+1/2}\left(\frac{e'-e^n}{\Delta t}\right)\right]-\frac{\alpha^n\varphi}{F_r^2}\frac{\partial G_a^n}{\partial x_a}, \tag{31}$$

and the fractional steps approximation of the energy balance (21), represented by

$$\rho^{n+1/2}\left(\frac{e'-e^n}{\Delta t}+\theta_1 u_b^n\frac{\partial e'}{\partial x_b}+\theta_2 u_b^n\frac{\partial e^n}{\partial x_b}\right)+\frac{\gamma}{RePr}\frac{\partial q_b^n}{\partial x_b}-\frac{\gamma Ec}{Re}\tau_{ab}^n\frac{\partial u_a^n}{\partial x_b}=0, \tag{32}$$

$$\rho^{n+1/2}\left(\frac{e^{n+1}-e'}{\Delta t}\right)+\left(\gamma-1+\gamma Ecp^{n+1}-\frac{\gamma Ec}{Fr^2}\rho^{n+1/2}\varphi\right)\frac{\partial u_b^n}{\partial x_b}=0. \tag{33}$$

In the above equations, the superscripts n and $n+1$ denote the time level and Δt is the time step. Here, the parameters θ_1 and $\theta_2=1-\theta_1$ control the implicitness in the time discretization of the convective term (explicit for $\theta_1=0$ and implicit for $\theta_1=1$). Unless otherwise stated, we shall employ $\theta_1=0.5$ in our computations.

The mass–velocity, pressure and internal energy fields at time level k are interpolated as $\hat{G}_a^k=N_jG_{aj}^k$, $\hat{p}^k=N_jp_j^k$ and $\hat{e}^k=N_je_j^k$ respectively, where N_j represents the linear Lagrangian shape functions and G_{aj}^k, p_j^k and e_j^k are the corresponding nodal values at time level k.

When splitting the energy balance into Equations (32) and (33), we have isolated the term representing the compressible contribution in Equation (33). Equation (32), on the other hand, retains the remaining terms, typical of incompressible applications.

From Equations (31) and (33), we obtain

$$\alpha^n\left(\frac{p^{n+1}-p^n}{\Delta t}\right)+\frac{\beta^n}{\rho^{n+1/2}}\left[\gamma-1+\gamma Ecp^{n+1}-\frac{\gamma Ec}{Fr^2}\rho^{n+1/2}\varphi\right]\frac{\partial u_a^n}{\partial x_a}+\frac{\partial G_a^{n+1}}{\partial x_a}$$
$$=\frac{\beta^n}{\rho^{n+1/2}}\left[\rho^{n+1/2}\left(\frac{e'-e^n}{\Delta t}\right)\right]-\frac{\alpha^n\varphi}{Fr^2}\frac{\partial G_a^n}{\partial x_a}. \tag{34}$$

Using the Galerkin method, we obtain the following weighted residual approximation of Equation (34):

$$\int_\Omega N_i\left(\frac{\alpha^n}{\Delta t}+\frac{\gamma Ec\beta^n}{\rho^{n+1/2}}\frac{\partial\hat{u}_b^n}{\partial x_b}\right)\hat{p}^{n+1}\,\mathrm{d}\Omega+\int_\Omega N_i\frac{\partial\hat{G}_a^{n+1}}{\partial x_a}\,\mathrm{d}\Omega$$
$$=\int_\Omega N_i\frac{\alpha^n}{\Delta t}\hat{p}^n\,\mathrm{d}\Omega+\int_\Omega N_i\frac{\beta^n}{\Delta t}(\hat{e}'-\hat{e}^n)\,\mathrm{d}\Omega+\int_\Omega N_i\left(\frac{\gamma Ec}{Fr^2}\varphi+\frac{1-\gamma}{\rho^{n+1/2}}\right)\beta^n\frac{\partial\hat{u}_a^n}{\partial x_a}\,\mathrm{d}\Omega$$
$$-\int_\Omega\frac{\alpha^n\varphi}{Fr^2}N_i\frac{\partial\hat{G}_a^n}{\partial x_a}\,\mathrm{d}\Omega,\quad\forall\ \text{free}\ p_i^{n+1}. \tag{35}$$

In the above equation, the weighting functions N_i are the shape functions associated with the free nodal pressure variables p_i^{n+1}. The density $\rho^{n+1/2}$ is computed as follows, using a Taylor series expansion from time level n and the mass balance,

$$\rho^{n+1/2}=\rho^n+\frac{\Delta t}{2}\frac{\partial\rho^n}{\partial t}=\rho^n-\frac{\Delta t}{2}\frac{\partial\hat{G}_a^n}{\partial x_a}, \tag{36}$$

while ρ^n, α^n and β^n are evaluated as constants within each finite element (they are obtained from the internal energy and pressure defined at the element baricentre).

Returning to Equation (35), let us now integrate by parts the mass–velocity divergence term

$$\int_\Omega N_i\frac{\partial\hat{G}_a^{n+1}}{\partial x_a}\,\mathrm{d}\Omega=-\int_\Omega\frac{\partial N_i}{\partial x_a}\hat{G}_a^{n+1}\,\mathrm{d}\Omega+\int_\Gamma N_i\hat{G}_a^{n+1}n_a\,\mathrm{d}\Gamma, \tag{37}$$

where n_a denotes the outward normal vector at the boundary Γ. Using a Taylor series in time and approximating the momentum balance (20), the above equation yields

$$\int_\Omega N_i\frac{\partial\hat{G}_a^{n+1}}{\partial x_a}\,\mathrm{d}\Omega=-\int_\Omega\frac{\partial N_i}{\partial x_a}\left(\hat{G}_a^n+\Delta t\frac{\partial\hat{G}_a^{n+\theta}}{\partial t}\right)\mathrm{d}\Omega+\int_\Gamma N_i\hat{G}_a^{n+1}n_a\,\mathrm{d}\Gamma$$
$$=\int_\Omega\Delta t\frac{\partial N_i}{\partial x_a}\left(\hat{u}_b^n\frac{\partial\hat{G}_a^n}{\partial x_b}+\frac{\partial\hat{u}_b^n}{\partial x_b}\hat{G}_a^n-\frac{1}{Re}\frac{\partial\hat{\tau}_{ab}^n}{\partial x_b}+(1-\Phi_1)\frac{\partial\hat{p}^{n+1}}{\partial x_a}-\frac{\Phi_1}{Fr^2}\rho^{n+1/2}g_a\right.$$
$$\left.+\Phi_2\frac{\partial\hat{e}^n}{\partial x_a}\right)\mathrm{d}\Omega-\int_\Omega\frac{\partial N_i}{\partial x_a}\hat{G}_a^n\,\mathrm{d}\Omega+\int_\Gamma N_i\hat{G}_a^{n+1}n_a\,\mathrm{d}\Gamma. \tag{38}$$

Note that the pressure gradient term, which arises from the momentum balance, is approximated with a fully implicit time discretization. Using integration by parts again,

$$\int_\Omega N_i \frac{\partial \hat{G}_a^{n+1}}{\partial x_a}\,\mathrm{d}\Omega = \int_\Omega N_i \frac{\partial \hat{G}_a^{n}}{\partial x_a}\,\mathrm{d}\Omega + \int_\Gamma N_i(\hat{G}_a^{n+1} - \hat{G}_a^{n}) n_a\,\mathrm{d}\Gamma + \int_\Omega \Delta t \frac{\partial N_i}{\partial x_a}\left(\hat{u}_b^n \frac{\partial \hat{G}_a^n}{\partial x_b} + \frac{\partial \hat{u}_b^n}{\partial x_b}\hat{G}_a^n - \frac{1}{Re}\frac{\partial \hat{\tau}_{ab}^n}{\partial x_b} + (1-\Phi_1)\frac{\partial \hat{p}^{n+1}}{\partial x_a} - \frac{\Phi_1}{Fr^2}\rho^{n+1/2} g_a + \Phi_2 \frac{\partial \hat{e}^n}{\partial x_a}\right)\mathrm{d}\Omega. \tag{39}$$

Boundary conditions for pressure and mass flux are prescribed on non-overlapping parts of the boundary Γ_p and Γ_G, such that $\Gamma_p \cup \Gamma_G = \Gamma$ and $\Gamma_p \cap \Gamma_G = \varnothing$, as

$$p = \bar{p} \quad \text{on } \Gamma_p, \tag{40}$$

$$G_a n_a = \bar{G} \quad \text{on } \Gamma_G. \tag{41}$$

It is important to recall that the weighting functions, N_i, are associated with the free pressure nodal values and thus vanish on the Γ_p part of the boundary, where pressure is prescribed. Thus, after considering the above boundary conditions, Equation (39) yields

$$\int_\Omega N_i \frac{\partial \hat{G}_a^{n+1}}{\partial x_a}\,\mathrm{d}\Omega = \int_\Omega N_i \frac{\partial \hat{G}_a^{n}}{\partial x_a}\,\mathrm{d}\Omega + \int_{\Gamma_G} N_i(\bar{G}^{n+1} - \bar{G}^{n})\,\mathrm{d}\Gamma + \int_\Omega \Delta t \frac{\partial N_i}{\partial x_a}\left(\hat{u}_b^n \frac{\partial \hat{G}_a^n}{\partial x_b} + \frac{\partial \hat{u}_b^n}{\partial x_b}\hat{G}_a^n - \frac{1}{Re}\frac{\partial \hat{\tau}_{ab}^n}{\partial x_b} + (1-\Phi_1)\frac{\partial \hat{p}^{n+1}}{\partial x_a} - \frac{\Phi_1}{Fr^2}\rho^{n+1/2} g_a + \Phi_2 \frac{\partial \hat{e}^n}{\partial x_a}\right)\mathrm{d}\Omega. \tag{42}$$

The boundary term in the above equation disappears if the specified mass flux on Γ_G does not vary in time. In particular, it vanishes at solid walls or when steady state solutions are sought.

Introducing Equation (42) back into the pressure equation (35), we obtain

$$\int_\Omega N_i\left(\frac{\alpha^n}{\Delta t} + \frac{\gamma Ec \beta^n}{\rho^{n+1/2}}\frac{\partial \hat{u}_b^n}{\partial x_b}\right)\hat{p}^{n+1}\,\mathrm{d}\Omega + \int_\Omega \Delta t(1-\Phi_1)\frac{\partial N_i}{\partial x_a}\frac{\partial \hat{p}^{n+1}}{\partial x_a}\,\mathrm{d}\Omega =$$

$$\int_\Omega N_i \frac{\alpha^n}{\Delta t}\hat{p}^n\,\mathrm{d}\Omega + \int_\Omega N_i \frac{\beta^n}{\Delta t}(\hat{e}' - \hat{e}^n)\,\mathrm{d}\Omega + \int_\Omega \Delta t \frac{\Phi_1}{Fr^2}\rho^{n+1/2}\frac{\partial N_i}{\partial x_a} g_a\,\mathrm{d}\Omega - \int_\Omega \Delta t \Phi_2 \frac{\partial N_i}{\partial x_a}\frac{\partial \hat{e}^n}{\partial x_a}\,\mathrm{d}\Omega$$
$$- \int_\Omega \Delta t \frac{\partial N_i}{\partial x_a}\left(\hat{u}_b^n \frac{\partial \hat{G}_a^n}{\partial x_b}\hat{G}_a^n\right)\mathrm{d}\Omega + \int_\Omega N_i\left(\frac{\gamma Ec}{Fr^2}\varphi + \frac{1-\gamma}{\rho^{n+1/2}}\right)\beta^n \frac{\partial \hat{u}_a^n}{\partial x_a}\,\mathrm{d}\Omega - \int_\Omega \frac{\alpha^n \varphi}{Fr^2} N_i \frac{\partial \hat{G}_a^n}{\partial x_a}\,\mathrm{d}\Omega$$
$$- \int_\Omega N_i \frac{\partial \hat{G}_a^n}{\partial x_a}\,\mathrm{d}\Omega - \int_{\Gamma_G} N_i(\bar{G}^{n+1} - \bar{G}^n)\,\mathrm{d}\Gamma, \quad \forall \text{ free } p_i^{n+1}. \tag{43}$$

The pressure equation (43) involves pressure terms arising from the mass, momentum and energy (compressible part) equations. Most importantly, these pressure terms are

approximated using a fully implicit time discretization, which introduces numerical damping of pressure errors. This permits retaining stability in the pressure computation, despite ignoring the short time scales associated to the fast pressure waves that characterize nearly incompressible flows.

It is important to note that before Equation (43) can be solved, one has to determine the internal energy field $\hat{e}'$ corresponding to the solution of Equation (32). This task, which can be regarded as a pre-processing for the pressure update, is described next.

The local residual of the incompressible part of the energy equation (32) is written as

$$\hat{r}_e = \hat{\rho}^{n+1/2}\left(\frac{\hat{e}' - \hat{e}^n}{\Delta t} + \theta_1 \hat{u}_b^n \frac{\partial \hat{e}'}{\partial x_b} + \theta_2 \hat{u}_b^n \frac{\partial \hat{e}^n}{\partial x_b}\right) + \frac{\gamma}{RePr}\frac{\partial \hat{q}_b^n}{\partial x_b} - \frac{\gamma Ec}{Re}\hat{\tau}_{ab}^n \frac{\partial u_a^n}{\partial x_b}, \tag{44}$$

where $\hat{e}' = N_j e_j'$.

The summation of squared residuals on the domain is given by

$$S = \int_\Omega \lambda \hat{r}_e \hat{r}_e \, \mathrm{d}\Omega. \tag{45}$$

For the time being we do not specify any particular spatial discretization for $\hat{q}_b$ and $\hat{\tau}_{ab}$ and treat the viscous and heat flux contributions as source terms at time level n.

Minimizing the squared residuals S with respect to the free nodal values e_i' and choosing $\lambda = \Delta t/\hat{\rho}^{n+1/2}$, we obtain the following Petrov–Galerkin weighted residual statement,

$$\begin{aligned}&\int_\Omega \left(N_i + \theta_1 \Delta t\, \hat{u}_c^n \frac{\partial N_i}{\partial x_c}\right)\frac{\hat{\rho}^{n+1/2}}{\Delta t}\left(\hat{e}' - \hat{e}^n + \theta_1 \Delta t\, \hat{u}_b^n \frac{\partial \hat{e}'}{\partial x_b} + \theta_2 \Delta t\, \hat{u}_b^n \frac{\partial \hat{e}^n}{\partial x_b}\right)\mathrm{d}\Omega \\ &+ \int_\Omega \left(N_i + \theta_1 \Delta t\, \hat{u}_c^n \frac{\partial N_i}{\partial x_c}\right)\left(\frac{\gamma}{RePr}\frac{\partial \hat{q}_b^n}{\partial x_b} - \frac{\gamma Ec}{Re}\hat{\tau}_{ab}^n \frac{\partial u_a^n}{\partial x_b}\right)\mathrm{d}\Omega = 0, \quad \forall \text{ free } e_i'.\end{aligned} \tag{46}$$

Note that the weighting function in Equation (46) has the same structure of the streamline upwind Petrov–Galerkin (SUPG) weighting function [6], but depends on the time step and on the degree of implicitness used. For $\theta_1 = 0.5$, an appropriate amount of *streamline upwinding* is introduced if one adjusts the time step according to the so-called *optimal upwind parameter* [6]. We shall return to this point in Section 3.4, when discussing the local time stepping procedure adopted in this work.

Internal energy and heat flux boundary conditions are prescribed on the boundary partitions Γ_e and Γ_q, such that $\Gamma_e \cup \Gamma_q = \Gamma$ and $\Gamma_e \cup \Gamma_q = \varnothing$, as

$$e = \bar{e} \quad \text{on } \Gamma_e, \tag{47}$$

$$q_b n_b = \bar{q} \quad \text{on } \Gamma_q. \tag{48}$$

Integrating by parts the Galerkin heat flux divergence term in Equation (46) and considering the above boundary conditions, we obtain

$$\int_\Omega \left(N_i + \theta_1 \Delta t\, \hat{u}_c^n \frac{\partial N_i}{\partial x_c}\right) \frac{\hat{\rho}^{n+1/2}}{\Delta t} \left(\hat{e}' + \theta_1 \Delta t\, \hat{u}_b^n \frac{\partial \hat{e}'}{\partial x_b}\right) \mathrm{d}\Omega$$
$$= \int_\Omega \left(N_i + \theta_1 \Delta t\, \hat{u}_c^n \frac{\partial N_i}{\partial x_c}\right) \frac{\hat{\rho}^{n+1/2}}{\Delta t} \left(\hat{e}^n - \theta_2 \Delta t\, \hat{u}_b^n \frac{\partial \hat{e}^n}{\partial x_b}\right) \mathrm{d}\Omega$$
$$+ \int_\Omega \left(N_i + \theta_1 \Delta t\, \hat{u}_c^n \frac{\partial N_i}{\partial x_c}\right) \frac{\gamma Ec}{Re}\, \hat{\tau}_{ab}^n \frac{\partial \hat{u}_a^n}{\partial x_b}\, \mathrm{d}\Omega + \int_\Omega \frac{\gamma}{RePr} \frac{\partial N_i}{\partial x_b}\, \hat{q}_b^n\, \mathrm{d}\Omega - \int_{\Gamma_q} \frac{\gamma}{RePr} N_i \bar{q}\, \mathrm{d}\Gamma$$
$$- \int_\Omega \theta_1 \Delta t\, \hat{u}_c^n \frac{\partial N_i}{\partial x_c} \frac{\gamma}{RePr} \frac{\partial \hat{q}_b^n}{\partial x_b}\, \mathrm{d}\Omega, \quad \forall \text{ free } e_i'. \tag{49}$$

At this point, we have to introduce the spatial discretization of the viscous and heat flux terms into Equation (49). Based on Equations (25) and (26), these quantities are expressed in terms of the discretized velocity and temperature fields as

$$\hat{\tau}_{ab}^n = -\frac{2}{3}\mu\left(\frac{\partial \hat{u}_c^n}{\partial x_c}\right)\delta_{ab} + \mu\left(\frac{\partial \hat{u}_a^n}{\partial x_b} + \frac{\partial \hat{u}_b^n}{\partial x_a}\right), \tag{50}$$

$$\hat{q}_b^n = -\kappa \frac{\partial \hat{T}^n}{\partial x_b}, \tag{51}$$

where $\hat{u}_a^n = N_j u_{aj}^n$ and $\hat{T}^n = N_j T_j^n$ are interpolated using the linear Lagrangian shape functions N_j and the nodal values for velocity and temperature,

$$T_j^n = e_j^n, \tag{52}$$

$$u_{aj}^n = \frac{G_{aj}^n}{\rho_j^n}. \tag{53}$$

In the above equation, ρ_j^n denotes the density nodal values. These are obtained through the state equation (27) using the corresponding nodal values for internal energy and pressure.

It is important to remark that with the above approximations for heat flux and viscous stress, the equivalence between Equation (49) and the least-squares method is lost. This is due to the occurrence, in Equations (44) and (45), of second-order derivatives of temperature (internal energy), which can be represented inside the finite elements, but not across element interfaces. In the formulation adopted here, the heat flux contributions to Equation (49) are evaluated on element interiors, following a procedure that has become standard in the context of Petrov–Galerkin formulations [8].

Note that the implementation of the least-squares method would require either recasting the problem in terms of first-order spatial differentials, with the introduction of new dependent variables, or employing C_1 shape functions. Although no longer equivalent to the least-squares method, the present Petrov–Galerkin formulation inherits from the former the important mathematical properties of *symmetry* and *positive definiteness*, while retaining the use of simple C_0 shape functions. It is also worth stressing that the formulation automatically introduces *streamline upwinding* [6], a feature of foremost importance as far as the simulation of convection dominated flows is concerned.

Once the internal energy $\hat{e}'$ is determined, the strongly implicit pressure equation (43) can be solved for $\hat{p}^{n+1}$. The next stage is the computation of the new mass–velocity $\hat{G}_a^{n+1}$ and the new internal energy $\hat{e}^{n+1}$. Again, Petrov–Galerkin weighted residual statements are employed in the discretization, as described in the following sections.

3.2. Mass–velocity update

The weighted residual statement used for the mass–velocity update is obtained using the same rationale employed in Section 3.1, when deriving the Petrov–Galerkin approximation of Equation (32). Here, the local residual of the momentum equation (20) is

$$\hat{r}_a = \frac{\hat{G}_a^{n+1} - \hat{G}_a^n}{\Delta t} + \hat{u}_b^n \frac{\partial \hat{G}_a^{n+\theta_1}}{\partial x_b} + \frac{\partial \hat{u}_b^n}{\partial x_b} \hat{G}_a^{n+\theta_1} - \frac{1}{Re} \frac{\partial \hat{\tau}_{ab}^n}{\partial x_b} + (1-\Phi_1) \frac{\partial \hat{p}^{n+1}}{\partial x_a} - \frac{\Phi_1}{Fr^2} \rho^{n+1/2} g_a + \Phi_2 \frac{\partial \hat{e}^n}{\partial x_a}, \tag{54}$$

where $\hat{G}_a^{n+\theta_1} = \theta_1 \hat{G}_a^{n+1} + \theta_2 \hat{G}_a^n$.

The summation of squared residuals on the domain is given by

$$S = \int_\Omega \lambda \hat{r}_a \hat{r}_a \, \mathrm{d}\Omega. \tag{55}$$

Minimizing the squared residuals with respect to the mass–velocity degrees of freedom G_a^{n+1} and choosing $\lambda = \Delta t$, we obtain the following weighted residual statement

$$\begin{aligned}
&\int_\Omega \left[\left(1 + \theta_1 \Delta t \frac{\partial \hat{u}_c^n}{\partial x_c} \right) N_i + \theta_1 \Delta t \, \hat{u}_c^n \frac{\partial N_i}{\partial x_c} \right] \frac{1}{\Delta t} \left[\left(1 + \theta_1 \Delta t \frac{\partial \hat{u}_b^n}{\partial x_b} \right) \hat{G}_a^{n+1} + \theta_1 \Delta t \, \hat{u}_b^n \frac{\partial \hat{G}_a^{n+1}}{\partial x_b} \right] \mathrm{d}\Omega \\
&= \int_\Omega \left[\left(1 + \theta_1 \Delta t \frac{\partial \hat{u}_c^n}{\partial x_c} \right) N_i + \theta_1 \Delta t \, \hat{u}_c^n \frac{\partial N_i}{\partial x_c} \right] \frac{1}{\Delta t} \left[\left(1 - \theta_2 \Delta t \frac{\partial \hat{u}_b^n}{\partial x_b} \right) \hat{G}_a^n - \theta_2 \Delta t \, \hat{u}_b^n \frac{\partial \hat{G}_a^n}{\partial x_b} \right] \mathrm{d}\Omega \\
&\quad + \int_\Omega \left[\left(1 + \theta_1 \Delta t \frac{\partial \hat{u}_c^n}{\partial x_c} \right) N_i + \theta_1 \Delta t \, \hat{u}_c^n \frac{\partial N_i}{\partial x_c} \right] \\
&\quad \times \left[\frac{1}{Re} \frac{\partial \hat{\tau}_{ab}^n}{\partial x_b} - (1-\Phi_1) \frac{\partial \hat{p}^{n+1}}{\partial x_a} + \frac{\Phi_1}{Fr^2} \hat{\rho}^{n+1/2} g_a - \Phi_2 \frac{\partial \hat{e}^n}{\partial x_a} \right] \mathrm{d}\Omega, \quad \forall \text{ free } G_{ai}^{n+1}.
\end{aligned} \tag{56}$$

Mass–velocity and traction boundary conditions are prescribed on the boundary partitions Γ_{G_a} and Γ_{t_a}, such that $\Gamma_{G_a} \cup \Gamma_{t_a} = \Gamma$ and $\Gamma_{G_a} \cup \Gamma_{t_a} = \varnothing$, as

$$G_a = \bar{G}_a \quad \text{on } \Gamma_{G_a}, \tag{57}$$

$$\left(-p\delta_{ab} + \frac{1}{Re} \tau_{ab} \right) n_b = \bar{t}_a \quad \text{on } \Gamma_{t_a}, \tag{58}$$

where δ_{ab} is the Kronecker delta. Using Green's identity on Equation (56) and considering the above boundary conditions, we obtain

$$\int_\Omega \left[\left(1+\theta_1\Delta t\,\frac{\partial \hat{u}_c^n}{\partial x_c}\right)N_i+\theta_1\Delta t\,\hat{u}_c^n\frac{\partial N_i}{\partial x_c}\right]\frac{1}{\Delta t}\left[\left(1+\theta_1\Delta t\,\frac{\partial \hat{u}_b^n}{\partial x_b}\right)\hat{G}_a^{n+1}+\theta_1\Delta t\,\hat{u}_b^n\frac{\partial \hat{G}_a^{n+1}}{\partial x_b}\right]\mathrm{d}\Omega =$$

$$\int_\Omega \left[\left(1+\theta_1\Delta t\,\frac{\partial \hat{u}_c^n}{\partial x_c}\right)N_i+\theta_1\Delta t\,\hat{u}_c^n\frac{\partial N_i}{\partial x_c}\right]\frac{1}{\Delta t}\left[\left(1-\theta_2\Delta t\,\frac{\partial \hat{u}_b^n}{\partial x_b}\right)\hat{G}_a^{n+1}-\theta_2\Delta t\,\hat{u}_b^n\frac{\partial \hat{G}_a^{n+1}}{\partial x_b}\right]\mathrm{d}\Omega$$
$$+\int_{\Gamma_{ta}} N_i\bar{t}_a\,\mathrm{d}\Gamma+\int_\Omega\frac{\partial N_i}{\partial x_a}\hat{p}^{n+1}\,\mathrm{d}\Omega+\int_\Omega\Phi_1 N_i\frac{\partial \hat{p}^{n+1}}{\partial x_a}\,\mathrm{d}\Omega-\int_\Omega\frac{1}{Re}\frac{\partial N_i}{\partial x_b}\hat{\tau}_{ab}^n\,\mathrm{d}\Omega$$
$$+\int_\Omega\theta_1\Delta t\left[\frac{\partial \hat{u}_c^n}{\partial x_c}N_i+\hat{u}_c^n\frac{\partial N_i}{\partial x_c}\right]\left[\frac{1}{Re}\frac{\partial \hat{\tau}_{ab}^n}{\partial x_b}-(1-\Phi_1)\frac{\partial \hat{p}^{n+1}}{\partial x_a}\right]\mathrm{d}\Omega$$
$$+\int_\Omega\left[\left(1+\theta_1\Delta t\,\frac{\partial \hat{u}_c^n}{\partial x_c}\right)N_i+\theta_1\Delta t\,\hat{u}_c^n\frac{\partial N_i}{\partial x_c}\right]\left[\frac{\Phi_1}{Fr^2}\hat{\rho}^{n+1/2}g_a-\Phi_2\frac{\partial \hat{e}^n}{\partial x_a}\right]\mathrm{d}\Omega,\quad\forall\ \text{free}\ G_{a_i}^{n+1}. \tag{59}$$

The above equation is solved for each mass–velocity component in turn ($\hat{G}_a^{n+1}$, for $a=1, nsd$), immediately after the pressure field has been determined.

3.3. Internal energy update

In Section 3.1, we have considered the energy balance in the form of Equation (21) rather than the form shown in Equation (22). This permitted including the compressible contribution to the energy balance (21) into the equation for pressure, as indicated by Equations (31)–(34). In order to update the internal energy field, though, we prefer to use the energy balance in the form of Equation (22), which allows the direct utilization of the newly computed mass–velocity $\boldsymbol{G}^{n+1}$.

The Petrov–Galerkin/least-squares based approach is also used to derive the scheme for energy update. Here, the local residual of the energy equation (22) is written as

$$\hat{r}_e=\gamma\hat{\rho}^{n+1/2}\left(\frac{\hat{e}^{n+1}-\hat{e}^n}{\Delta t}+\hat{u}_b^n\frac{\partial \hat{e}^{n+\theta_1}}{\partial x_b}\right)+\frac{\gamma}{RePr}\frac{\partial \hat{q}_b^n}{\partial x_b}-\frac{\gamma Ec}{Re}\hat{\tau}_{ab}^n\frac{\partial \hat{u}_a^n}{\partial x_b}$$
$$-\gamma Ec\left[\frac{\hat{p}^{n+1}-\hat{p}^n}{\Delta t}+(1-\Phi_1)\hat{u}_b^n\frac{\partial \hat{p}^{n+1}}{\partial x_b}+\left(\frac{1-\Phi_1}{Fr^2}\right)\hat{G}_b^{n+1}g_b+\Phi_2\hat{u}_b^n\frac{\partial \hat{e}^n}{\partial x_b}+\frac{\varphi}{Fr^2}\frac{\partial \hat{G}_b^{n+1}}{\partial x_b}\right], \tag{60}$$

and the summation of squared residuals on the domain is given by

$$S=\int_\Omega\lambda\hat{r}_e\hat{r}_e\,\mathrm{d}\Omega. \tag{61}$$

Minimizing the squared residuals S with respect to the free nodal values e_i^{n+1} and considering the boundary conditions given by Equations (47) and (48), we obtain

$$\int_\Omega \left(N_i + \theta_1 \Delta t\, \hat{u}_c^n \frac{\partial N_i}{\partial x_c}\right)\gamma \frac{\hat{\rho}^{n+1/2}}{\Delta t}\left(\hat{e}^{n+1} + \theta_1 \Delta t\, \hat{u}_b^n \frac{\partial \hat{e}^{n+1}}{\partial x_b}\right) \mathrm{d}\Omega =$$

$$\int_\Omega \left(N_i + \theta_1 \Delta t\, \hat{u}_c^n \frac{\partial N_i}{\partial x_c}\right)\gamma \frac{\hat{\rho}^{n+1/2}}{\Delta t}\left(\hat{e}^{n} - \theta_2 \Delta t\, \hat{u}_b^n \frac{\partial \hat{e}^{n}}{\partial x_b}\right) \mathrm{d}\Omega + \int_\Omega \frac{\gamma}{RePr}\frac{\partial N_i}{\partial x_b}\hat{q}_b^n \,\mathrm{d}\Omega$$
$$- \int_\Omega \frac{\gamma}{RePr} N_i \bar{q}\, \mathrm{d}\Gamma + \int_\Omega \left(N_i + \theta_1 \Delta t\, \hat{u}_c^n \frac{\partial N_i}{\partial x_c}\right)\frac{\gamma Ec}{Re}\hat{\tau}_{ab}^n \frac{\partial \hat{u}_a^n}{\partial x_b}\,\mathrm{d}\Omega -$$

$$\int_{\Gamma_q} \frac{\gamma}{RePr}\theta_1 \Delta t\, \hat{u}_c^n \frac{\partial N_i}{\partial x_c}\frac{\partial \hat{q}_b^n}{\partial x_b}\,\mathrm{d}\Omega + \int_\Omega \left(N_i + \theta_1 \Delta t\, \hat{u}_c^n \frac{\partial N_i}{\partial x_c}\right)\gamma Ec\left[\frac{\hat{p}^{n+1} - \hat{p}^n}{\Delta t} + (1-\Phi_1)\hat{u}_b^n \frac{\partial \hat{p}^{n+1}}{\partial x_b}\right]$$
$$\times \mathrm{d}\Omega + \int_\Omega \left(N_i + \theta_1 \Delta t\, \hat{u}_c^n \frac{\partial N_i}{\partial x_c}\right)\gamma Ec\left[\left(\frac{1-\Phi_1}{Fr^2}\right)\hat{G}_b^{n+1} g_b + \Phi_2\, \hat{u}_b^n \frac{\partial \hat{e}^n}{\partial x_b} + \frac{\varphi}{Fr^2}\frac{\partial \hat{G}_b^{n+1}}{\partial x_b}\right]\mathrm{d}\Omega,$$

$$\forall \text{ free } e_i^{n+1}. \tag{62}$$

3.4. Local time stepping

The choice of time step is of foremost importance for the accuracy and stability of the method. Note that the Petrov–Galerkin weightings, and the associated stabilization terms, are parameterized by the time step. The stabilization terms can be also interpreted as *artificial dissipation*. Here, though, such terms arise naturally from the derivation, rather than being added *a posteriori*.

For linear elements, a proper amount of *streamline upwinding* is introduced in the momentum balance choosing the time step as

$$\Delta t = \left[\coth\left(\frac{C_{Re}}{2}\right)\frac{2}{C_{Re}}\right]\frac{h_e}{\|\mathbf{u}^n\|}, \tag{63}$$

where $\|\mathbf{u}^n\|$ is the velocity modulus and h_e is the characteristic element size (the square root of the element area). The element Reynolds number C_{Re} and the problem Reynolds number Re are related as follows:

$$C_{Re} = \frac{\rho\,\|\mathbf{u}^n\| h_e}{\mu} Re. \tag{64}$$

It is important to recall that the variables and governing equations have been non-dimensionalized. Thus, the time step, velocity, physical properties and element size in Equations (63) and (64) are non-dimensional quantities. The corresponding dimensional values can be readily obtained using the reference scales for length (L), velocity (u_0), density (ρ_0), viscosity (μ_0) and time (L/u_0).

The above time step choice is appropriate to follow the time evolution of the momentum convection–diffusion processes resolvable in a mesh with size h_e, as argued by De Sampaio *et al.* [9]. Indeed, Equation (63) gives for the pure convection limit, i.e. $C_{Re} \to \infty$,

$$\Delta t = \frac{h_e}{\|\mathbf{u}^n\|}, \tag{65}$$

whereas for pure diffusion ($C_{Re} = 0$) it yields

$$\Delta t = \frac{1}{6} \frac{\rho h_e^2}{\mu} Re. \tag{66}$$

The relationship between the time step given by Equation (63), also called the *intrinsic time scale*, and the modelling (filtering) of the subgrid scales was investigated in a recent paper by Hughes [10].

On the other hand, to introduce optimal upwinding in the fluid energy equation we have to replace the element Reynolds number in Equation (63) by the element Peclet number,

$$C_{Pe} = \frac{\rho \|\mathbf{u}^n\| h_e}{\kappa} RePr. \tag{67}$$

Clearly, the time scales for the momentum and energy equations may differ. Furthermore, note that the time step given by Equation (63) varies spatially according to local values of velocity, physical properties and mesh size. Thus, if optimal *upwinding* is to be introduced in both momentum and energy balances, we need to consider two distinct spatially varying time step distributions.

We employ here an algorithm that allows each degree of freedom to advance in time according to its own local time step, while interpolated results are periodically output at fixed times [11]. The algorithm starts with all degrees of freedom *active* and with variables defined at time t^n. Then, it proceeds as follows:

(a) Set element time steps for mass–velocity using the corresponding C_{Re} and element time steps for internal energy and pressure using the corresponding C_{Pe}.
(b) Project the element time step values onto mesh nodes, obtaining nodal time step distributions for $\hat{G}_a$, $\hat{p}$ and $\hat{e}$.
(c) Choose an interpolation time step Δt_{int} between the minimum ($\Delta t_{\min}$) and the maximum ($\Delta t_{\max}$) time scales.
(d) Define the interpolation time level $t_{\text{int}} = t^n + \Delta t_{\text{int}}$.
(e) Solve sequentially Equations (49), (43), (59) and (62) for the *active* degrees of freedom using the respective nodal time step distributions.
(f) Interpolate, on the time domain, the degrees of freedom whose tracked time have exceeded t_{int} and freeze their interpolated values at t_{int}. These degrees of freedom are temporarily removed from the list of *active* variables and treated as *pseudo* boundary conditions for the problem defined in terms of the remaining *active* variables.

(g) Are there any active variables left?
If yes
g1) Recompute the local time steps for the remaining *active* variables and return to step (e).
Else
g2) Output the solution at t_{int}.
g3) Release the *inactive* (frozen) degrees of freedom.
g4) Redefine $t^n = t_{\text{int}}$ and return to step (a).
End if

The process continues until the required analysis time interval has been covered. Note that the extra bookkeeping needed for tracking each degree of freedom time *position* pays off in computational effort, for degrees of freedom associated with larger time steps are updated less frequently than those associated to smaller ones. The algorithm described above leads to a weighting function adaptive method, where the local time step is adjusted according to the local velocity, physical properties and mesh size, aiming to optimize the approximation on a given mesh.

3.4.1. Neglecting the pressure time scale in nearly incompressible flows. The time scales associated with pressure transients have not been considered when defining the local time steps. In fact, we are only concerned with the time scales of the momentum and energy transfers that occur through convection–diffusion processes. However, as the incompressible limit is approached ($M \ll 1$), pressure waves travel much faster than the flow itself. In such a case, pressure transients occur much faster than we are able to capture and stability will depend on the algorithm's ability to damp the corresponding pressure errors.

For schemes that approximate pressure explicitly, ignoring the pressure time scales leads to instability. However, that is not the case for the present method: the pressure terms in the pressure equation (43) are approximated using a fully implicit time discretization. This permits stability to be retained, despite neglecting the short time scales associated with fast pressure waves.

3.5. Adaptive remeshing

A remeshing scheme concerns only the spatial discretization. However, when dealing with transient processes, the overall error in the solution is associated not only with the spatial discretization, but also with the time integration of the governing equations. Thus, some form of time step adaptation is necessary, as far as a transient analysis is concerned.

In this work, the *a posteriori* error estimator proposed by Zienkiewicz and Zhu [12] is used to estimate the velocity gradient error and to guide the remeshing. The scheme is designed to generate meshes containing a controlled number of elements, in such a way that the velocity gradient error becomes evenly distributed. The remeshing procedure is fully automatic and triggered during a transient analysis whenever the relative variation of the estimated error exceeds a preset value [13].

The local time stepping algorithm is used in conjunction with the remeshing scheme. This permits linking spatial and time step refinement through Equation (63) and naturally leads to

a simultaneous time–space adaptive procedure. Indeed, whenever the remeshing scheme creates some local refinement to better resolve a particular flow feature, the time step distribution is also adapted accordingly, so that the corresponding time evolution can be appropriately followed.

It is important to remark that although our formulation is formally $O(\Delta t)$, the use of the time–space adaptive procedure allows for the local refinement of the time step itself. As a consequence, despite the formal first-order accuracy, our procedure can lead to better time discretizations than methods showing a formal higher-order accuracy, but which assume a constant time step throughout the analysis domain.

4. NUMERICAL EXAMPLES

The formulation presented in the previous sections has been applied to the analysis of some representative internal and external flows, covering a wide range of Mach numbers. The thermodynamic and transport properties of air were used in all examples. Sutherland's formula [14] was used to compute the viscosity and a constant Prandtl number of 0.72 was assumed.

4.1. Circular cylinder in cross-flow

We consider here the problem of a circular cylinder in cross-flow. This is a transient, nearly incompressible, external flow application. The Reynolds and Mach numbers for the analysis are based on the free-stream conditions. The cylinder diameter D is used as reference length.

Experiments show that a steady state solution, with symmetric vortices appearing behind the cylinder, occurs up to $Re = 40$. For laminar flows at higher Reynolds numbers, there is a periodic shedding of vortices, forming what is called a Von Karmann vortex street [15]. The frequency f of the periodic flow is non-dimensionalized by the Strouhal number $St = f D/u_0$. Hammache and Gharib [16] obtained experimentally the relation $St = 0.212 - 5.35/Re$ between the Strouhal and the Reynolds numbers.

A numerical simulation for $Re = 100$ and $M = 0.1$ was performed. The meshes in the beginning of the analysis typically have 2000 elements. However, as the periodic flow is established, the number of elements in the adaptive meshes increases to about 5000 elements, becoming nearly constant thereafter.

Figure 1 shows the periodic vortex shedding behind the cylinder. Figure 2 presents two typical adapted meshes generated during the transient simulation. The oscillation frequency f obtained from the numerical analysis yields a Strouhal number $St = 0.160$, in good agreement with the value of $St = 0.158$ predicted by the experimental correlation [16].

4.2. Thermal stratification in a square cavity

Air is initially at rest and thermal equilibrium, at temperature $\theta_0 = 300$ K and atmospheric pressure, when the temperatures at the left and right vertical walls are suddenly modified to $\theta_L = 301.5$ K and $\theta_R = 298.5$ K respectively. The horizontal walls are considered adiabatic and no-slip boundary conditions are applied to all solid boundaries.

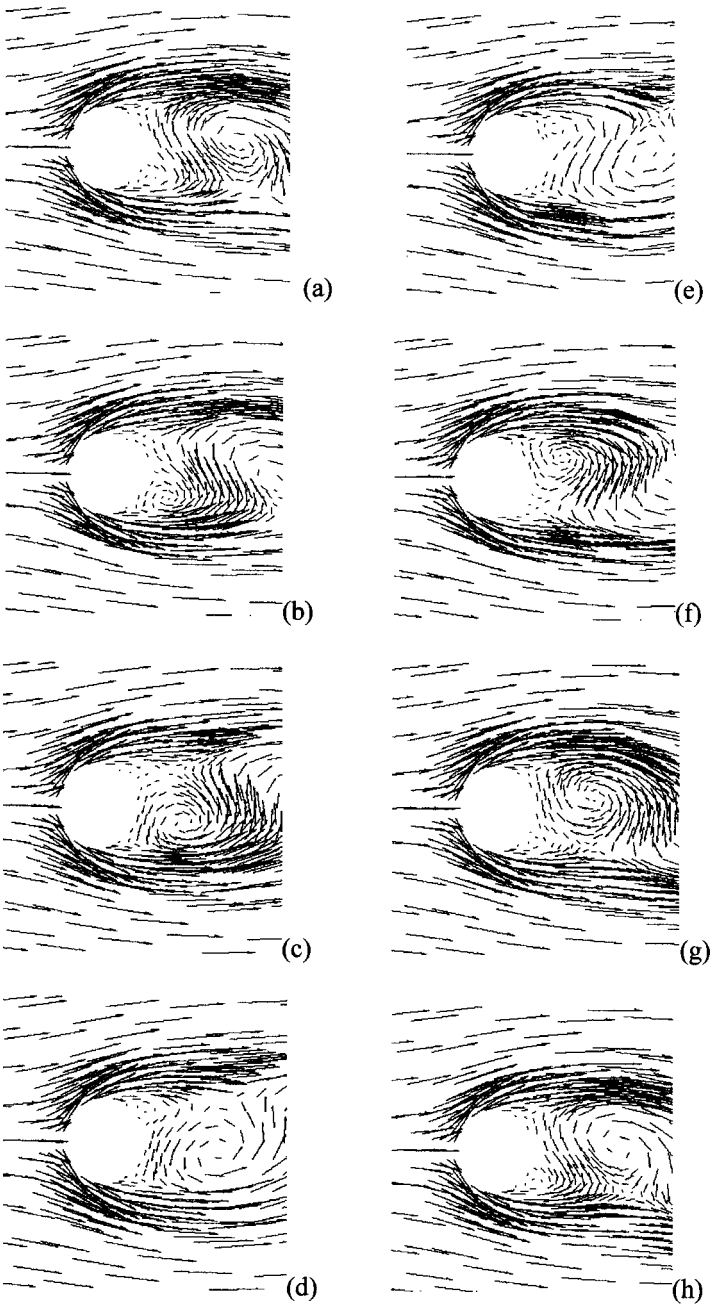

Figure 1. Periodic formation of vortices behind a circular cylinder in cross-flow for $Re = 100$ and $M = 0.1$.

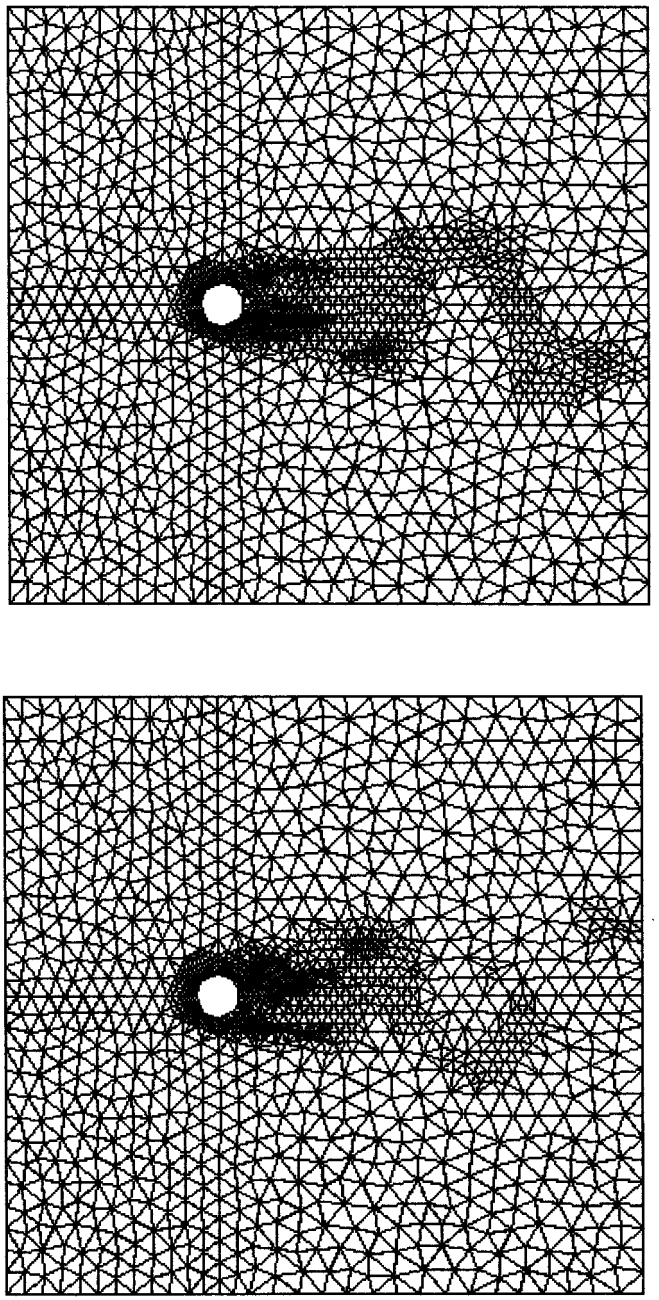

Figure 2. Typical adapted meshed generated in the simulation of the cylinder in cross-flow problem.

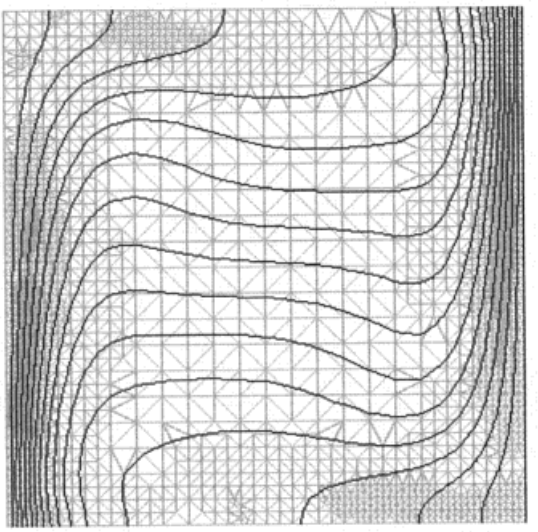

(a)

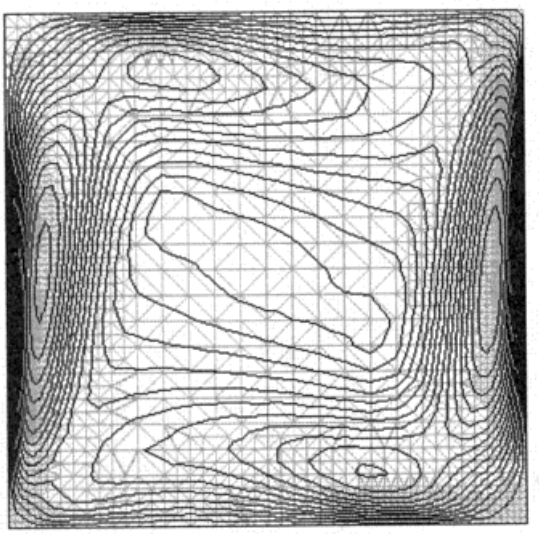

(b)

Figure 3. Thermal stratification in a square cavity ($GrPr = 10^5$ and $Pr = 0.72$): (a) temperature contours; (b) Mach number contours.

The imposed temperature boundary conditions induce buoyancy forces and lead to a free convection stratified flow inside the cavity. Results are parameterized by the Grashof ($Gr = \rho_0^2|\mathbf{g}|\beta_v\Delta\theta L^3/\mu_0^2$) and Prandtl numbers. The height of the cavity is chosen as the characteristic length L. The reference thermodynamic and transport properties are those corresponding to the initial state.

Figure 3 shows temperature and Mach number contours for $GrPr = 10^5$ and $Pr = 0.72$, after the steady state has been reached. The final adaptive mesh contains 2947 nodes and 5636 elements. Note that the maximum local Mach number in this analysis was as low as 1.35×10^{-4}.

Heat transfer data is presented in the form of the Nusselt number. This is given by $Nu = q''_w L/k_0\Delta\theta$, where q''_w is the wall heat flux. Figure 4 shows the Nusselt number distribution along the cold wall at steady state. The average value $\overline{Nu}$ obtained in our computation is 4.47936, which is close to the benchmark value [17] of 4.52188.

4.3. Compressible flow around an NACA0012 airfoil

We consider here two examples of external compressible flow around a NACA0012 airfoil. In both cases, the reference properties and the reference velocity are those corresponding to the free stream. The airfoil chord is chosen as the characteristic length L.

4.3.1. Transonic flow. The first example is a transonic flow with $M = 0.85$, $Re = 500$ and 0° incidence. A fixed mesh, refined close to the airfoil surface, was used in this steady state analysis. Local time steps were computed as described in Section 3.4. However, as we were

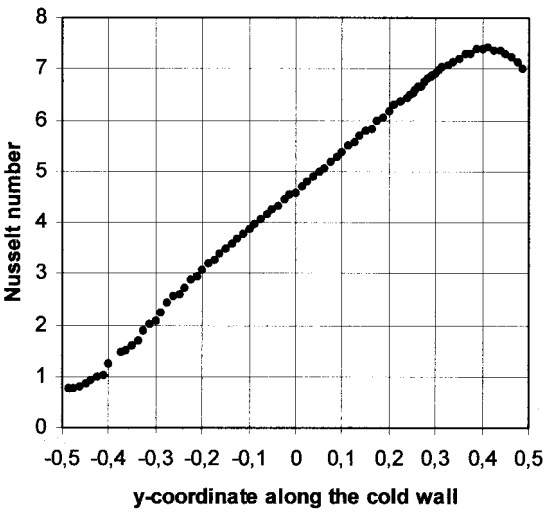

Figure 4. Thermal stratification in a square cavity ($GrPr = 10^5$ and $Pr = 0.72$): Nusselt number distribution along the cold wall.

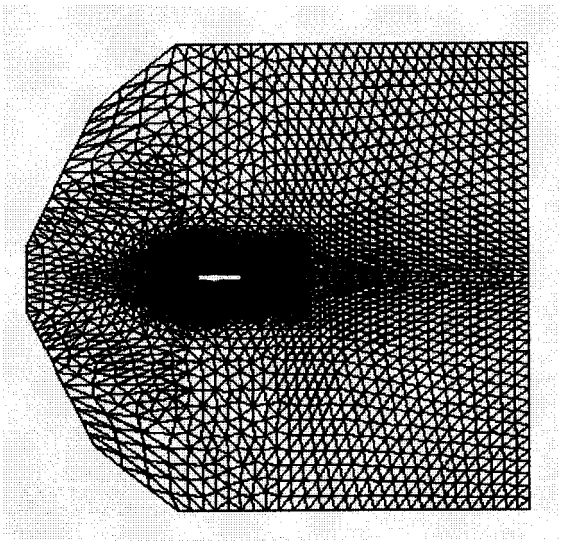

Figure 5. Flow around an NACA0012 airfoil with $M = 0.85$, $Re = 500$ and 0° incidence: fixed mesh containing 5328 nodes and 10238 elements.

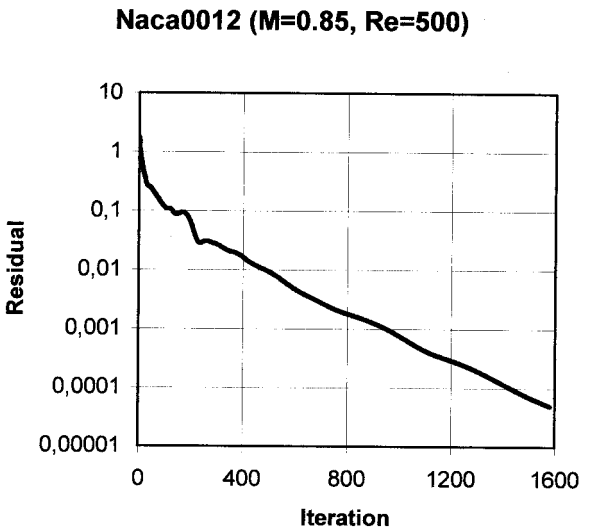

Figure 6. Flow around an NACA0012 airfoil with $M = 0.85$, $Re = 500$ and 0° incidence: convergence history.

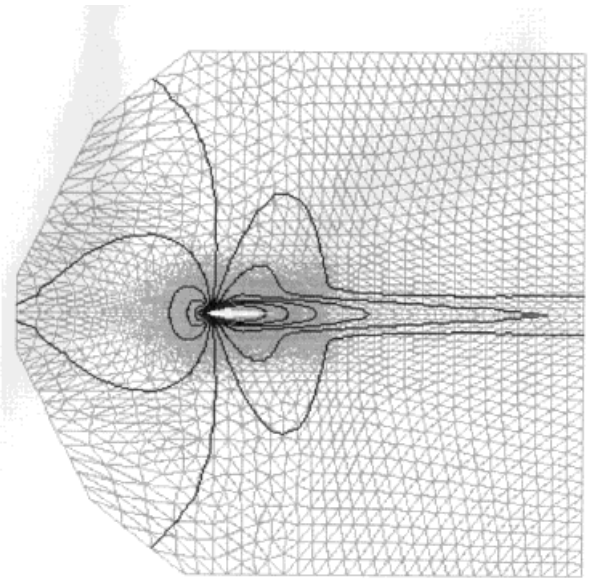

(a)

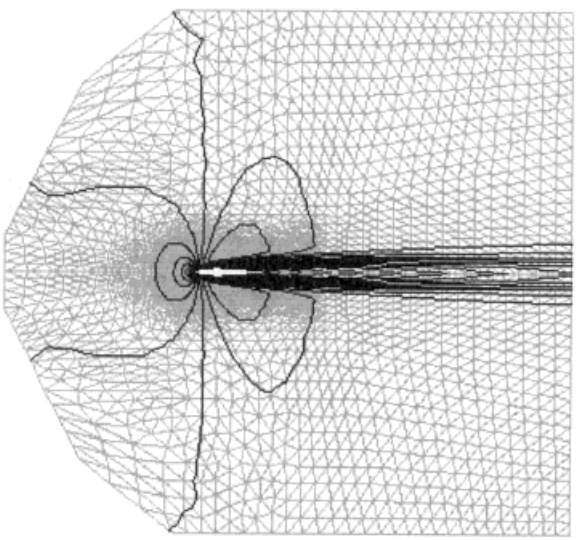

(b)

Figure 7. Flow around an NACA0012 airfoil with $M = 0.85$, $Re = 500$ and 0° incidence: (a) density contours; (b) Mach number contours.

interested in steady state results only, the computation was allowed to proceed freely, without resorting to time interpolation.

Mass–velocity and temperature are imposed as boundary conditions at the inflow boundary while pressure is imposed at the outflow. At the airfoil surface, the no-slip velocity condition is applied together with a uniform temperature corresponding to the free-stream stagnation value.

The mesh employed is depicted in Figure 5. The minimum element size is 0.004 L. The convergence towards the steady state solution is presented in Figure 6. Figure 7 shows the density and Mach number contours. The friction coefficient along the chord is depicted in Figure 8. This result is in good agreement with the friction coefficient presented by Nigro *et al.* [18] and Shakib [19].

4.3.2. Supersonic flow. The second example is a supersonic flow at $M = 2.0$, $Re = 106$ and 10° incidence. Mass–velocity, temperature and pressure are imposed at the supersonic inflow boundary. The no-slip velocity condition is applied at the airfoil surface, which is assumed adiabatic. No boundary conditions are imposed at the supersonic outflow.

In this example, we have performed a transient, time–space adaptive computation. Here, the remeshing procedure was employed to construct meshes according to the estimated error on velocity gradients, while local time steps were adjusted according to the resulting element sizes and physical conditions. The time interpolation algorithm described in Section 3.4 was employed to synchronize the computation.

The transient was run from $t^* = 0$ to $t^* = 10$. At $t^* = 10$, the computation is virtually at steady state, with a residual of 0.001. Figure 9 shows the analysis domain and the final adaptive mesh containing 7266 nodes and 14185 elements. The minimum element size is

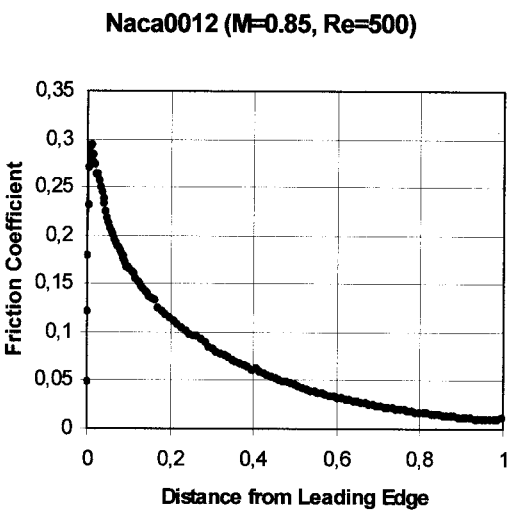

Figure 8. Flow around an NACA0012 airfoil with $M = 0.85$, $Re = 500$ and 0° incidence: friction coefficient along the chord.

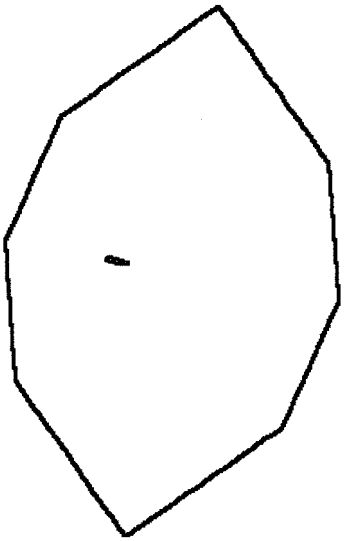

(a)

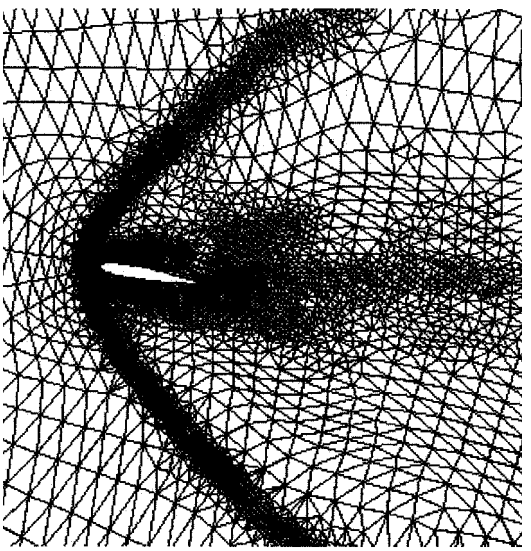

(b)

Figure 9. Flow around an NACA0012 airfoil with $M = 2$, $Re = 106$ and 0° incidence: (a) analysis domain; (b) detail of the mesh close to the airfoil.

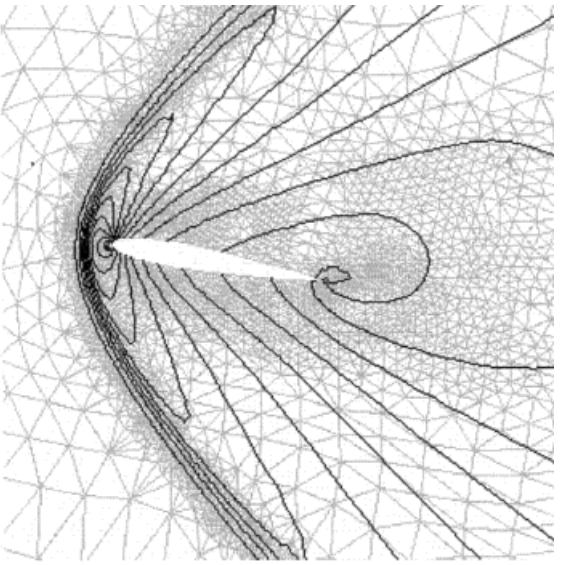

(a)

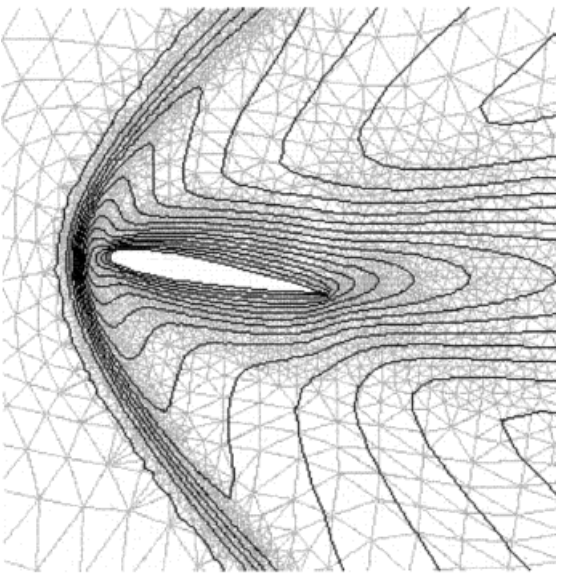

(b)

Figure 10. Flow around an NACA0012 airfoil with $M = 2$, $Re = 106$ and 10° incidence: (a) density contours; (b) Mach number contours.

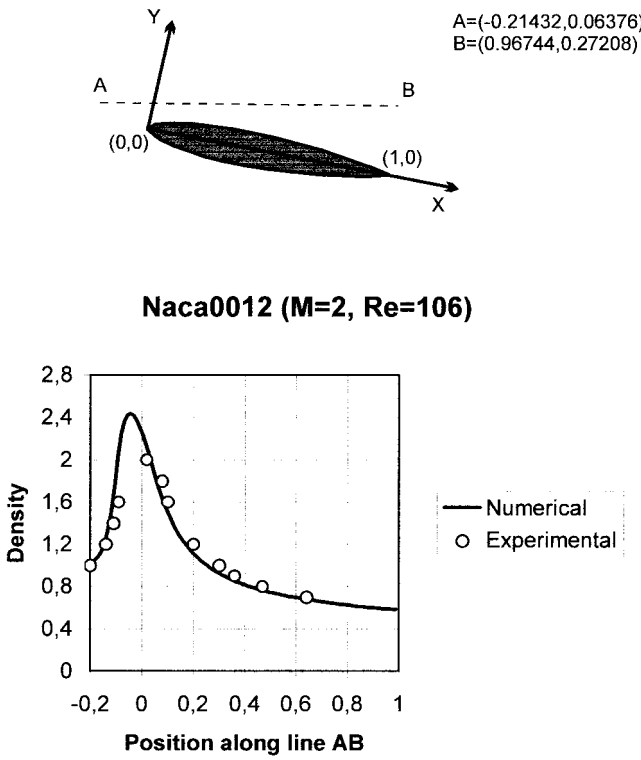

Figure 11. Flow around an NACA0012 airfoil with $M = 2$, $Re = 106$ and 10° incidence: comparison between numerical and experimental density data [20].

0.01 L. In particular, note the refinement on the regions comprising the frontal shock and the boundary layer. Density and Mach number contours on the vicinity of the airfoil are shown in Figure 10. Figure 11 presents a comparison between the computed density field and the corresponding experimental data obtained by Allègre *et al.* [20]. The comparison is made on the straight line AB, shown in Figure 11, which runs through the shock into the rarefaction zone. Note the good agreement between the numerical and the experimental density data.

5. CONCLUDING REMARKS

A new finite element formulation designed for the analysis of both compressible and nearly incompressible fluid dynamics has been presented. The method has shown good performance in the solution of some representative internal and external flows, ranging from the subsonic to the supersonic regime.

In particular, it has been possible to simulate some very small Mach number flows, without resorting to the incompressible model, and thus retaining the state equation of the fluid. This

is an attractive feature of the present formulation, as we intend to use it for the analysis of two-phase steam/water flows, where preserving the fluid thermodynamic relations is of foremost importance.

The numerical methods presented herein for two-dimensional laminar flows naturally extend for the analysis of three-dimensional problems and for the computation of turbulent flows with the Reynolds-averaged equations.

REFERENCES

1. K.C. Karki and S.V. Patankar, 'Pressure based calculation procedure for viscous flows at all speeds in arbitrary configurations', *AIAA J.*, **27**, 1167–1174 (1989).
2. C.R Maliska and A.F.C. Silva, 'A boundary-fitted finite volume method for the solution of compressible and/or incompressible fluid flows using both velocity and density corrections', *7th International Conference on Finite Element Flow Problems*, Huntsville, AL, 3–7 April 1989, pp. 405–412.
3. K.H. Chen and R.H. Pletcher, 'Primitive variable, strongly implicit calculation procedure for viscous flows at all speeds', *AIAA J.*, **29**, 1241–1249 (1991).
4. J.L.F. Azevedo and R.J. Martins, 'Compressible and incompressible flow simulations using a finite difference method', *Proc. 5th Int. Symp. on Computational Fluid Dynamics*, Sendai, Japan, 1993, pp. 38–43.
5. O.C. Zienkiewicz and R Codina, 'A general algorithm for compressible and incompressible flow. Part I: the split, characteristic-based scheme', *Int. J. Numer. Methods Fluids*, **20**, 869–885 (1995).
6. A. Brooks and T.J.R. Hughes, 'Streamline upwind/Petrov–Galerkin formulations for convection dominated flows with particular emphasis on the incompressible Navier–Stokes equations', *Comput. Methods Appl. Mech. Eng.*, **32**, 199–259 (1982).
7. P.A.B. De Sampaio and A.L.G.A. Coutinho, 'Parallel/vector finite element simulation of coupled flow and heat transfer', *Proc. 16th Iberian Latin American Conference on Computational Methods for Engineering*, Curitiba, Brazil, 1995, pp. 1401–1410.
8. T.J.R. Hughes, 'Recent progress in the development and understanding of SUPG methods with special reference to the compressible Euler and Navier–Stokes equations', *Int. J. Numer. Methods Fluids*, **7**, 1261–1275 (1987).
9. P.A.B. De Sampaio, P.R.M. Lyra, K. Morgan and N.P. Weatherill, 'Petrov–Galerkin solutions of the incompressible Navier–Stokes equations in primitive variables with adaptive remeshing', *Comput. Methods Appl. Mech. Eng.*, **106**, 143–178 (1993).
10. T.J.R Hughes, 'Multiscale phenomena: Green's functions, subgrid scale models, bubbles, and the origins of stabilized methods', *Proc. 9th Int. Conf. on Finite Elements in Fluids*, Venezia, Italia, 1995, pp. 99–114.
11. P.A.B. De Sampaio, 'Transient solutions of the incompressible Navier–Stokes equations in primitive variables employing optimal local time stepping', in C. Taylor (ed.), *Proc. 8th Int. Conf. on Numerical Methods for Laminar and Turbulent Flow*, vol. 8, Pineridge Press, Swansea, UK, 1993, pp. 1493–1504.
12. O.C. Zienkiewicz and J.Z. Zhu, 'A simple error estimator and adaptive procedure for practical engineering analysis', *Int. J. Numer. Methods Eng.*, **24**, 337–357 (1987).
13. P.A.B. De Sampaio and A.L.G.A. Coutinho, 'Simulation of free and forced convection incompressible flows using an adaptive parallel/vector finite element procedure', *Int. J. Numer. Methods Fluids*, **29**, 289–309 (1999).
14. C. Hirsch, *Numerical Computation of Internal and External Flows*, vol. 1, Wiley, New York, 1988.
15. RD. Blevins, *Flow Induced Vibrations*, Van Nostrand Reinhold, New York, 1977.
16. M. Hammache and M. Gharib, 'An experimental study of the parallel and oblique vortex shedding from circular cylinders', *J. Fluid Mech.*, **232**, 567–590 (1991).
17. M. Hortmann, M. Perić and G. Scheuerer, 'Multigrid benchmark solutions for laminar natural convection flows in square cavities', in I. Celik and C.J. Freitas (eds.), *Benchmark Test Cases for Computational Fluid Dynamics*, ASME, New York, 1990, pp. 1–6.
18. N. Nigro, M. Sorti and S. Idelsohn, 'GMRES physics-based preconditioner for all Reynolds and Mach numbers: numerical examples', *Int. J. Numer. Methods Fluids*, **25**, 1347–1371 (1997).
19. F. Shakib, 'Finite element analysis of the compressible Euler and Navier–Stokes equations', *Ph.D. Thesis*, Stanford University, 1988.
20. J. Allègre, M. Raffin and J.C. Lengrand, 'Experimental flowfields around NACA0012 airfoils located in subsonic and supasonic rarefied air streams', in M.O. Bristeau, R. Glowinski, J. Periaux and H. Viviand (eds.), *Numerical Simulation of Compressible Navier–Stokes Flows*, *A GAMM-Workshop*, *Notes on Numerical Fluid Dynamics*, vol. 18, 1987, pp. 59–68.

